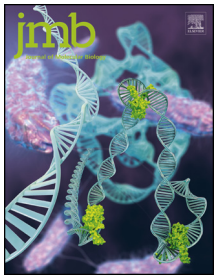

Crystallographic Analysis of the Catalytic Mechanism of Phosphopantothenoylcysteine Synthetase from *Saccharomyces cerevisiae*

Peiyi Zheng, Mengying Zhang, Muhammad Hidayatullah Khan, Hejun Liu, Yuping Jin, Jian Yue, Yongxiang Gao, Maikun Teng, Zhongliang Zhu and Liwen Niu

Hefei National Laboratory for Physical Sciences at Microscale, *School of Life Sciences, University of Science and Technology of China, 96 Jinzhai Road, Hefei, Anhui 230026, China*

Correspondence to Mengying Zhang, Zhongliang Zhu and Liwen Niu: *mengying@mail.ustc.edu.cn, zlzhu63@ustc.edu.cn, lwniu@ustc.edu.cn*
https://doi.org/10.1016/j.jmb.2019.01.012
Edited by Georg Schulz

Abstract

Phosphopantothenoylcysteine (PPC) synthetase (PPCS) catalyzes nucleoside triphosphate-dependent condensation reaction between 4′-phosphopantothenate (PPA) and L-cysteine to form PPC in CoA biosynthesis. The catalytic mechanism of PPCS has not been resolved yet. Coenzyme A biosynthesis protein 2 (Cab2) possesses activity of PPCS in *Saccharomyces cerevisiae*. Our enzymatic assays suggest that Cab2 could utilize both ATP and CTP to activate PPA *in vitro*. The results of isothermal titration calorimetry indicate that PPA, CTP, and ATP could bind to Cab2 individually, with PPA having the highest binding affinity. To provide further insight into the catalytic mechanism of Cab2, we determined the crystal structures of Cab2 and its complex with PPA, the reaction intermediate 4′-phosphopantothenoyl-CMP, the final reaction product PPC, and the product analogue phosphopantothenoylcystine. Except for PPA, all other ligands were generated *in situ* and present in the active-site pocket of Cab2. Structures of Cab2 in complex with ligands provide insight into substrates binding and its catalytic mechanism. Analysis of structures indicates that the carboxyl of PPA-moiety of ligands and the γ-amino group of Asn97 possess different conformations in these complex structures. The cysteine/cystine/serine selectivity assays for Cab2 indicate that the amino group rather than the thiol group of L-cysteine attacks the carbonyl of 4′-phosphopantothenoyl-CMP to form PPC. Based on structural and biochemical data, the catalytic mechanism of Cab2 was proposed for the first time.

Introduction

CoA is an essential cofactor that as an acyl carrier in almost all living organisms [1]. CoA and its derivative play an important role in more than 100 metabolic reactions, including synthesis and oxidation of fatty acid, synthesis of amino acid, and many other metabolic pathways [2]. CoA is biosynthesized from pantothenate, ATP, and L-cysteine using five-step enzymatic reaction catalyzed by pantothenate kinase (PANK), phosphopantothenoylcysteine (PPC) synthetase (PPCS), PPC decarboxylase, phosphopantetheine adenylyl transferase (PPAT), and dephosphocoenzyme A kinase (DPCK) [3]. Some of the CoA biosynthetic enzymes were found to be associated with different diseases, such as neurodegeneration with brain iron accumulation and autosomal-recessive dilated cardiomyopathy [4,5]. The CoA biosynthetic pathway is highly conserved among all organisms including both prokaryotes and eukaryotes.

PPCS catalyzes the second step of CoA biosynthesis, the formation of PPC from 4′-phosphopantothenate (PPA) and L-cysteine. It can be grouped into two distinct types based on the usage of nucleoside triphosphate. The PPCS enzyme, first characterized in *Escherichia coli* was reported as a CTP-dependent enzyme. This kind of PPCS, which usually fused to PPC decarboxylase and form bifunctional enzyme called CoaBC, mainly exists in prokaryotes. They transform PPA into 4′-phosphopantothenoyl-cytidylate via CTP [6,7]. The other type of PPCS mostly found in eukaryotes is carried out by monofunctional enzyme, which can activate PPA by using ATP or CTP [8–10]. Olzhausen *et al.* [11] reported that the products of yeast genes *CAB1, CAB2, CAB3, CAB4*, and *CAB5* have the

activities of PANK, PPCS, PPC decarboxylase, PPAT, and DPCK, respectively. Moreover, coenzyme A biosynthesis protein (Cab) 2, Cab3, Cab4, and Cab5 can interact with each other in yeast, which is obviously different from the CoA biosynthetic enzymes in other organisms [12]. The kinetic study of PPCS from *Enterococcus faecalis* suggests that the mechanism of PPCS can be classified as Bi Uni Uni Bi ping pong, with CTP binding, followed sequentially by PPA binding, pyrophosphate releasing, L-cysteine binding, PPC releasing, and CMP releasing [13].

To date, human monofunctional PPCS (PDB ID: 1P9O), PPCS domain of *E. coli* bifunctional enzyme CoaBC (ecCoaB, PDB ID: 1U7U), and monofunctional enzyme from *Streptococcus pneumoniae* (PDB ID: 2GK4) have been resolved [14,15]. Moreover, the structure of *Mycobacterium smegmatis* PPCS in complex with CTP (PDB ID: 4QJI) and ecCoaB in complex with CMP (PDB ID: 1U80), CTP (PDB ID: 1U7W), and 4′-phosphopantothenoyl-CMP (PMT; PDB ID: 1U7Z) have also been determined [15]. However, structures of PPCS in complex with PPA and PPC remain unexplored yet. Therefore, the catalytic mechanism of PPCS remains unclear. There are few literatures on the formation of PPC from the acyl-intermediate and L-cysteine. It is unclear whether the thiol of cysteine attacks the activated carboxyl to generate a thioester intermediate followed by an intramolecular S → N acyl shift to form PPC or the amino group of cysteine attacks the activated acyl group directly [16].

To address the catalytic mechanism of PPCS, we determined crystal structures of Cab2 in complex with substrate PPA, reaction intermediate PMT, reaction product PPC, and phosphopantothenoylcystine (PPS; PPC analogue). In the present study, the binding affinities of CTP, ATP, and PPA toward wild-type Cab2 were measured by isothermal titration calorimetry (ITC) assays. Enzymatic assays indicate that both ATP and CTP could be utilized by Cab2 to activate PPA *in vitro*. Crystallographic analysis reveals different conformations of the carboxyl of PPA-moiety and γ-amino group of the residue Asn97 in these ligands complex structures. Based on these results, catalytic mechanism for Cab2 was proposed.

Results and Discussion

Binding affinities of PPA and CTP to PPCS enzymes

The K_D for CTP binding to PPCS from *E. faecalis* was determined as 645 μM [13]. However, it is unclear whether the PPA can bind to PPCS independently of CTP and the affinity of PPA to PPCS has not been determined yet. To obtain insight into the substrate binding and to gain impartial binding affinities of PPA and CTP/ATP toward PPCS, we employed the ITC experiments with wild-type PPCS enzymes from yeast and *E. coli*, respectively. PPA binds to PPCS enzymes with high affinities, with the dissociation constants K_D PPA value ranging from 0.18 to 0.38 μM, whereas CTP binds with weaker affinities, with the K_D CTP value ranging from 2.00 to 5.63 μM (Fig. 1a–b, S1). The binding affinity for ATP to Cab2 was measured as a K_D of 0.71 μM, which was approximately 8-fold higher than that of CTP and about 4-fold weaker than PPA (Fig. 1a–c). Interestingly, PPA has the higher binding affinity for both PPCS enzymes as compared to ATP or CTP. Detailed thermodynamic parameters are listed in Table S1. Binding of ligands to Cab2 and ecCoaB were predominantly driven by enthalpy term with opposite contributions from entropy term (Table S1). The negative enthalpy changes suggest that the binding interactions are exothermic. The negative entropy change for PPA binding to Cab2 (*versus* positive entropy change of PPA binding to ecCoaB) might be due to additional hydrogen bond interactions observed in the $Cab2_{H337A}$–PPA complex structure. The results of ITC demonstrate that PPA, CTP, and ATP could bind to Cab2 independently, and the foremost has the highest binding affinity. This is different from the findings of Yao *et al.*, [13] who reported that binding of CTP to PPCS is prerequisite to PPA binding in *E. faecalis*. However we cannot exclude the possibility that CTP may bind prior to PPA in the presence of divalent metal ion. Further kinetics study is needed to validate the binding order of PPA and CTP.

Ligands specificity of Cab2

To determine the metal selectivity, the activity of Cab2 was measured in the presence 1 mM of various metals (Mg^{2+}, Mn^{2+}, Cu^{2+}, Ca^{2+}, and Fe^{3+}). We found that the enzymatic activity was supported by both Mg^{2+} and Mn^{2+}, which was consistent with previous report that Mg^{2+} or Mn^{2+} are required for PPCS activity (Fig. 1d) [9]. The enzymatic activity for Mn^{2+} was determined about 6% higher than Mg^{2+}. In addition, the Ca^{2+} involved assay displayed only about 5% activity of the Mg^{2+} involved assay.

Previous researchers have suggested that human PPCS can utilize both CTP and ATP to activate PPA [9]. To investigate the nucleotide selectivity of Cab2, the enzymatic activity was measured in the presence of 2 mM CTP or ATP. As shown in Fig. 1e, the CTP containing reaction showed about 69% of the activity of the ATP containing reaction. Similar to human PPCS, our results suggested that Cab2 can also use both ATP and CTP to activate PPA with preference for ATP [9].

In order to further identify the L-cysteine/cystine/serine selectivity of Cab2, Cab2 was assayed in the presence of 5 mM L-cysteine, cystine, or serine.

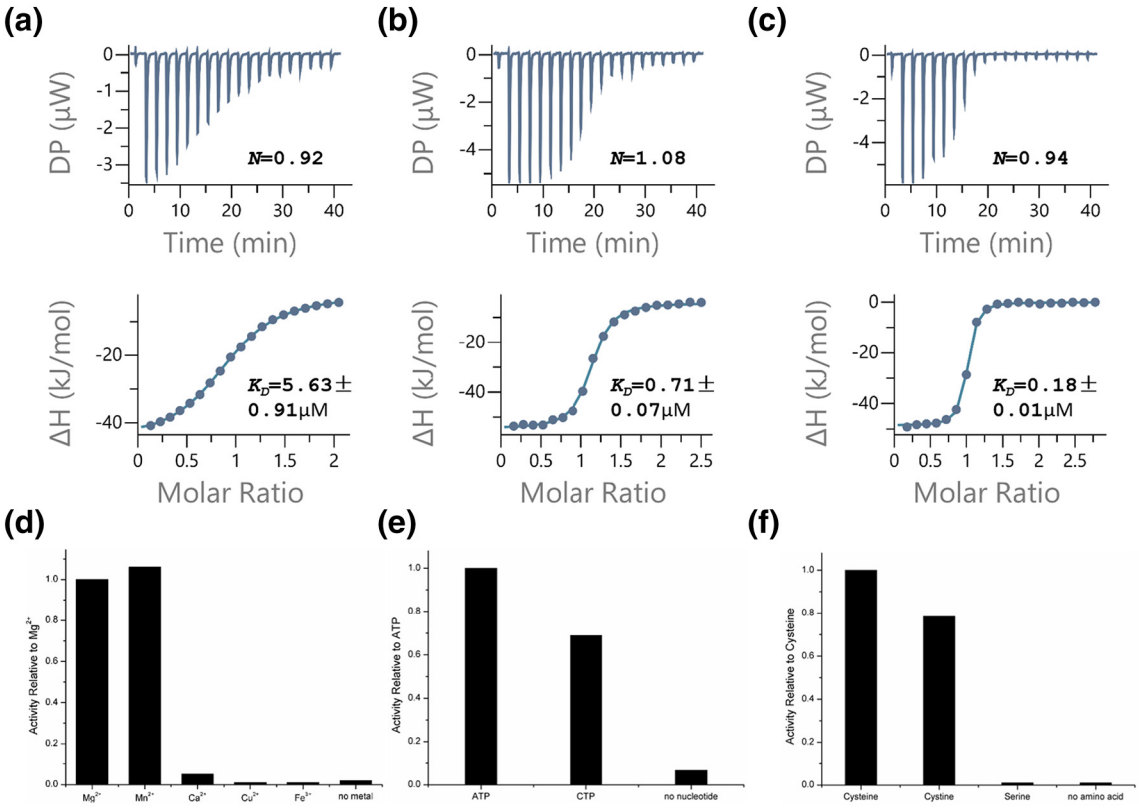

Fig. 1. Cofactor binding and ligands specificity of Cab2. (a) ITC measurement of the interaction between CTP and Cab2. (b) ITC measurement of the interaction between ATP and Cab2. (c) ITC measurement of the interaction between PPA and Cab2. (d) Metal ion dependence of Cab2. (e) ATP/CTP specificity of Cab2. (f) Cysteine/Cystine/Serine selectivity of Cab2.

Interestingly, the assay containing cystine showed 78.5% of the activity of the assay containing cysteine under otherwise same condition, which indicated that Cab2 could also utilize cystine *in vitro* (Fig. 1f). In contrast, the serine-containing reaction showed no detectable activity, which is in agreement with the findings of Strauss and Begley [17] that *E. coli* PPCS is highly selective for cysteine *versus* serine.

Overall structure of $Cab2_{H337A}$ is similar to other PPCS proteins

In order to understand the detail catalytic mechanism of Cab2, a series of crystallization experiments were performed. To overcome the twinning problem of wild type, the His337Ala mutant was used for crystallization throughout the study. The structures of $Cab2_{H337A}$ and its complex with PPA, PMT, PPC, and PPS were determined in our study. Initial phases of structures were determined by the molecular replacement method using human PPCS (PDB ID: 1P9O) as a search model [14]. Data collection and model refinement statistics of the structures are shown in Tables 1 and S2. The complex structure of PPA binding to $Cab2_{H337A}$ was resolved as a result of making the efforts to crystalize $Cab2_{H337A}$ in complex with PPA and CTP. Ligands of PMT, PPC, and PPS were generated *in situ*. The crystals of structures belong to monoclinic space group $p2_1$ with two monomers in the asymmetric unit (Fig. 2a). It should be noted that there were no significant conformational changes among the monomers of the five structures, with an overall RMSD of below 0.36 Å over the C^{α} atoms (Table S3). Each monomer of $Cab2_{H337A}$ adopts a typical α–β–α sandwich architecture that has a central eight-stranded β sheets (β5 ↑ β4 ↑ β1 ↑ β6 ↑ β9 ↑ β10 ↑ β11 ↓ β12 ↑) flanked by four α helices (α2, α6, α7, and α8) on one side and two α helices (α3 and α9) on the other side (Figs. 2a and S2), which is in agreement with the findings of Manoj *et al.* [14] and Stanitzek *et al.* [15] [14,15].

Active-site pocket of Cab2

Active-site pocket of Cab2 is located at the C-terminus of central parallel four-stranded β sheets, which is consistent with previously reported ecCoaB and human PPCS pockets (Fig. 2b) [14,15]. One wall of the pocket is formed by β9–loop–α8 and

Table 1. Data collection and refinement statistics.

	APO	PPA	PMT	PPC	PPS
Data collection					
Space group	$p2_1$	$p2_1$	$p2_1$	$p2_1$	$p2_1$
Unit cell parameters					
a, *b*, *c* (Å)	*a* = 53.79, *b* = 113.23, *c* = 57.78	*a* = 51.70, *b* = 113.52, *c* = 57.78	*a* = 51.76, *b* = 112.51, *c* = 55.78	*a* = 51.70, *b* = 113.56, *c* = 55.79	*a* = 51.10, *b* = 112.47, *c* = 54.57
β (°)	93.33	91.12	91.56	91.31	91.12
Resolution range (Å)	50.00–2.30	50.00–2.10	50.00–1.85	50.00–2.05	50.00–2.00
Unique reflections	30,686	36,076	46,177	40,365	30,667
Average redundancy	5.5 (5.2)	3.0 (2.3)	5.6 (5.2)	6.4 (5.6)	6.5 (5.7)
Completeness (%)	99.7 (99.9)	97.2 (96.8)	98.7 (97.9)	99.8 (99.5)	96.2 (95.8)
R_{merge} (%)[a]	7.7 (41.1)	8.7 (38.3)	9.4 (70.7)	9.1 (59.6)	11 (60.4)
$I/\sigma(I)$	16.3 (3.7)	11.4 (2.6)	13.9 (3.0)	18.1 (2.8)	16.7 (2.9)
Refinement statistics					
Resolution range (Å)	50.00–2.30	50.00–2.10	50.00–1.85	50.00–2.05	50.00–2.00
R_{factor} (%)[b]	18.39	20.3	17.8	17.7	18.1
R_{free} (%)[c]	24.60	24.8	21.9	21.5	21.8
RMSD bond lengths (Å)	0.0085	0.097	0.0139	0.007	0.0089
RMSD bond angles (°)	1.3301	1.3043	1.5005	1.2224	1.4146
Mean *B* factors (Å^2)					
Protein	64.5	33.0	36.8	42.5	32.8
Ligand	73 (GOL)/76(SO_4^{2-})	23.2	42.7	41.9	40.4
Water	60.2	37.6	41.8	49.8	40.0
Ramachandran plot[d]					
Favored (%)	97.4	97.9	97.5	97.5	98.0
Outliers (%)	0	0	0	0	0
PDB entry	6AI8	6AI9	6AIK	6AIM	6AIP

APO, ligand-free structure; PPA, structure of $Cab2_{H337A}$–PPA; PMT, structure of $Cab2_{H337A}$–PMT; PPC, structure of $Cab2_{H337A}$–PPC; PPS, structure of $Cab2_{H337A}$–PPS.

[a] Rmerge = $\sum_{hkl}\sum_i | I_i(hkl) - I(hkl) | / \sum_{hkl}\sum_i I_i(hkl)$, where $I_i(hkl)$ is the intensity of *i*th observation and $<I(hkl)>$is the mean value for reflection *hkl*.

[b] Rwork = $\sum_{hkl} || F_{obs}| - |F_{cacl} || / \sum_{hkl} |F_{obs}|$, where F_{obs} and F_{calc} are the observed and calculated structure-factor amplitudes, respectively.

[c] R_{free} is calculated same as R_{work} with 5% reflections, which were selected randomly from the refinement process.

[d] The categories were defined by PROCHECK.

β10–loop2. The loop2, represents connection of the central strand β10 and β11 sheets, which is essential for PPA binding. Another wall is formed by β3–loop–α3, loop–α7, C terminus of β1 and β6, and loops following them. The last wall of the pocket comprises loop1 and loop–β3, which are extending from the adjacent monomer. The loop1 connecting strand β6 and β7 is partially positioned as a disorder loop near the active-site cavity. The partially disordered loop is proposed to be important for the enzymatic reaction [15].

Binding of PPA to Cab2

The structure of $Cab2_{H337A}$ in complex with PPA shows unambiguous density for PPA in the conserved pocket (Fig. 2c, d). The phosphate group of PPA binds at the N terminus of helix α3 and C-terminus of loop2. The guanidine group of Arg313 is located at the phosphate group binding site that is mainly composed of backbone amides of Gly101 and Arg103, as well as side chains of Ser80, Ser99, and Thr102. Residues Phe98, Leu282, and Leu310 from one monomer and Val92 from the adjacent monomer including methyl groups of PPA form a hydrophobic core, which makes contributions in binding with substrate. Asn308 of β10 and Arg103 of helix α3 interact with the hydroxyl and carbonyl groups of PPA via three hydrogen bonds. The imino and carboxyl groups of PPA are immobilized by the protein backbone. The carboxyl group also forms a water-mediated hydrogen bond through W1 (water 612 in monomer A and water 644 in monomer B) with the γ-amino of Asn97. Compared with ecCoaB, the phosphate group of PPA is immobilized by two extra hydrogen bonds donated by guanidine group of Arg313, which is consistent with the larger negative entropy change for PPA binding to Cab2 (*versus* positive entropy for PPA binding to ecCoaB) (Table S1) [15]. We solved the complex structure of PPA rather than CTP with $Cab2_{H337A}$ by incubating the protein with PPA and CTP, which was in agreement with the higher binding affinity of PPA to Cab2 than CTP.

Binding of PMT to Cab2

To acquire the crystal of $Cab2_{H337A}$–PMT, several kinds of metal ions (Mg^{2+}, Mn^{2+}, Co^{3+}, Fe^{3+}, Cu^{2+}, Ca^{2+}) were incubated separately with the mixture of

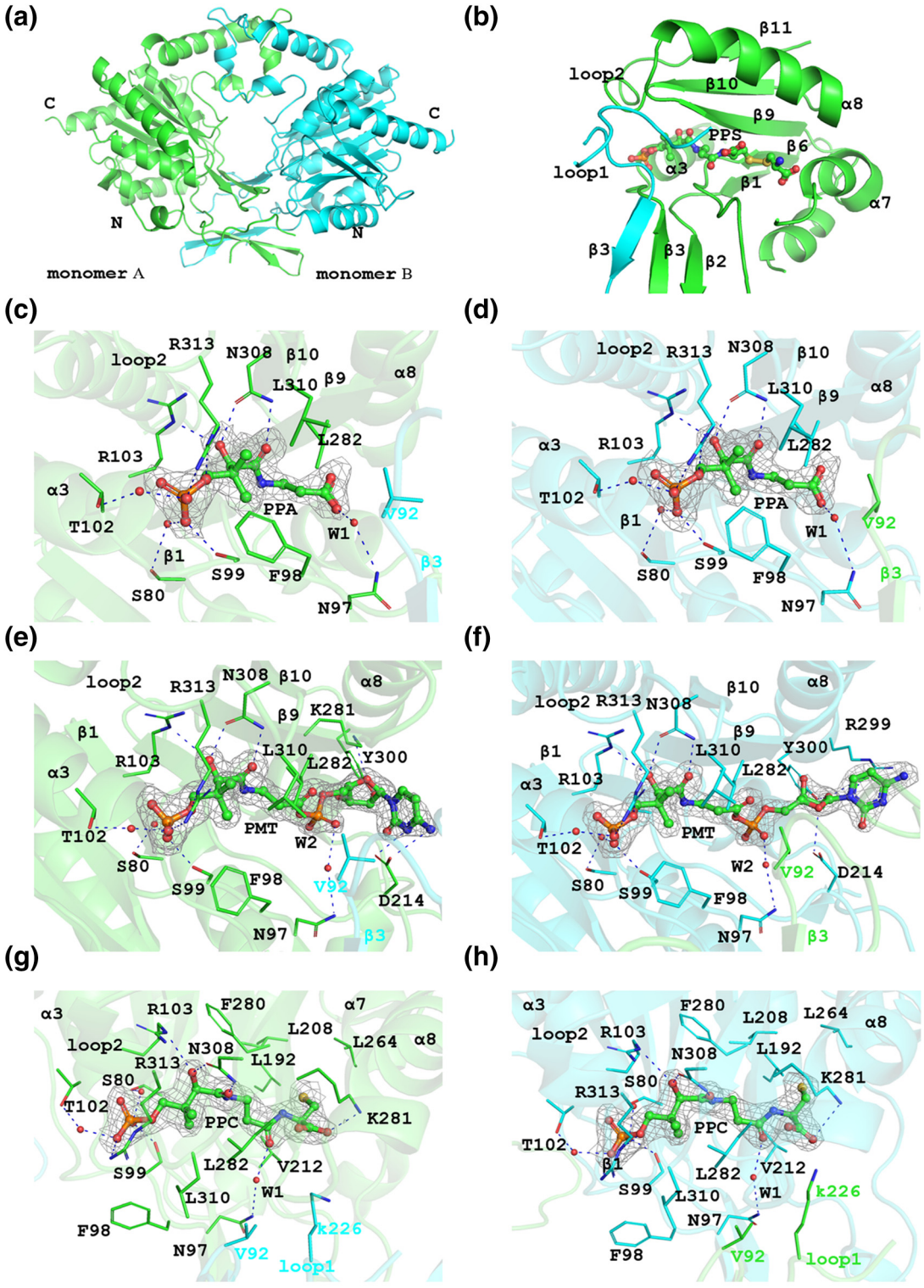

Fig. 2. Overall structure and active-site pocket of $Cab2_{H337A}$ and binding of PPA, PMT, and PPC. The secondary structure elements of monomer A are colored in green and monomer B in cyan. The ligands and the side chains of ligand-binding residues are shown as sticks. Dashed lines represent hydrogen bonds. (a) Overall structure of $Cab2_{H337A}$. (b)The active-site pocket of $Cab2_{H337A}$ in complex with PPS. (c and d) PPA recognition. The $2F_o - F_c$ electron density map is contoured at 0.8σ around PPA at the radius of 1.6 Å. (e and f) Binding interaction with PMT. The $2F_o - F_c$ electron density map is contoured at 0.8σ around PMT. (g and h) Binding interaction with PPC. The $2F_o - F_c$ electron density map is contoured at 0.8σ around PPC.

protein, PPA, and CTP for about 2 h [15]. The PMT containing complex crystal was obtained only in the presence of Mn^{2+}. However, the density for Mn^{2+} was absent from PMT complex structure. Our results indicate that Mn^{2+} might be essential for the crystallization of PMT complex with $Cab2_{H337A}$ but is not essential for PMT binding in yeast. The PPA-moiety (except the carboxyl) of PMT locates at the same position as the PPA molecule in $Cab2_{H337A}$–PPA complex structure and has the same interactions with

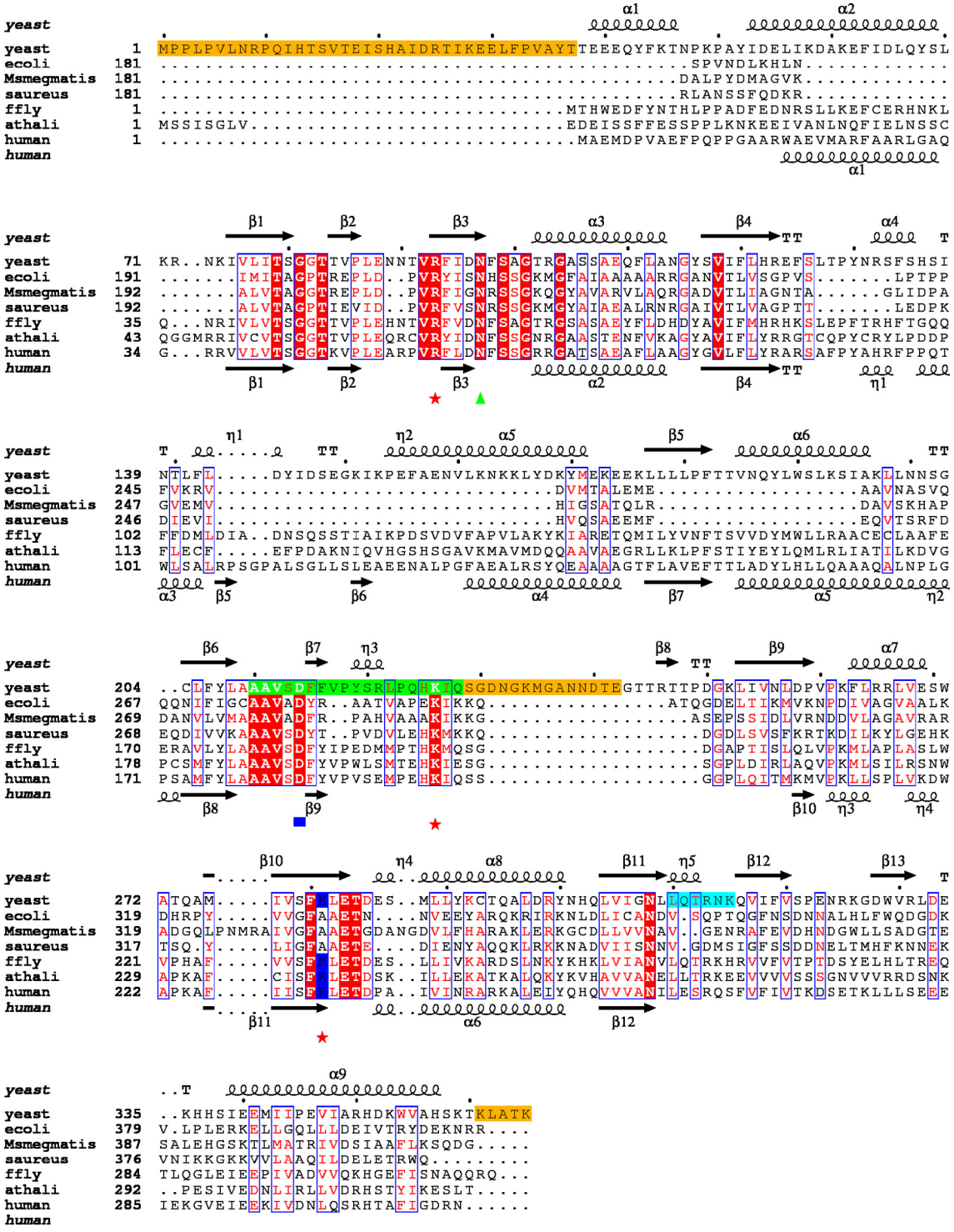

Fig. 3 (*legend on next page*)

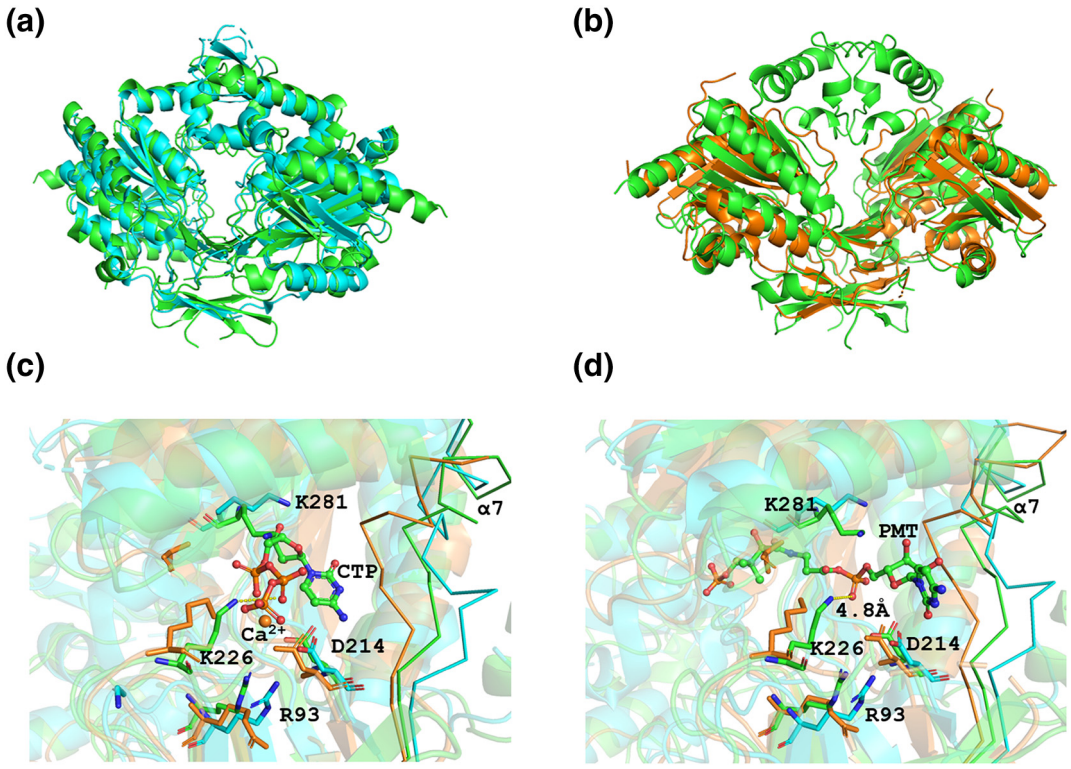

Fig. 4. Comparison of $Cab2_{H337A}$ with PPCS enzymes from human and *E. coli*. Superposed the structures of $Cab2_{H337A}$ to (a) human PPCS (PDB ID: 1P9O) and (b) ecCoaB (PDB ID: 1U7U) [14,15]. The dimers are colored with green for $Cab2_{H337A}$, cyan for human PPCS and orange for ecCoaB. (c) Comparison of the nucleotide binding sites of $Cab2_{H337A}$ with human PPCS (PDB ID: 1P9O) and ecCoaB-CTP (PDB ID: 1U7W). The CTP ligand is shown as ball and stick. (d)Comparison of the nucleotide binding sites of $Cab2_{H337A}$–PMT with human PPCS (PDB ID: 1P9O) and ecCoaB (PDB ID: 1U7W).

the protein (Fig. 2e, f). The γ-amino group of Asn97 forms a water-mediated hydrogen bond through W2 (water 633 in monomer A and water 664 in monomer B) with the α-phosphate of CMP-moiety rather than the carboxyl-moiety in PPA complex, which indicates that Asn97 might contribute in the formation of PMT. The CMP-moiety is anchored at the C terminus of strand β9 of the αβ-module. The ribose and cytosine groups are obviously flexible in the structure (Fig. S3). The cytosine interacts mainly with the side chain of Asp214 in monomer A while Arg299 in monomer B. The binding site of ribose group is mainly formed by the side chains of Lys281 and Tyr300 in monomer A, while Arg299 and Tyr300 in monomer B. The ribose and cytosine groups of CMP-moiety shows different conformations in PMT complex structure, which indicates that PMT is flexible and unstable.

Binding of PPC to Cab2

To address the catalytic mechanism of PPC synthesis, we resolved the structure of PPC in complex with $Cab2_{H337A}$. It is clear from Fig. 2g and h that the PPA moiety lies at the identical position as the PPA molecule in $Cab2_{H337A}$–PPA complex structure and has the same interactions with the protein. The L-cysteine-moiety attaches to the middle of strand β9 sheet. The ε-amino of Lys281 donates hydrogen bond to the carboxyl of L-cysteine-moiety, while ε-amino of Lys226 from the adjacent monomer forms a salt bridge

Fig. 3. Sequence alignment of Cab2 with other PPCS enzymes from selected organisms. The sequences were aligned with *ClustalW2* tool [18], and the figure was prepared using *ESPript*3.1 [19]. The sequences are listed for yeast, *E. coli*, *M. smegmatis*, *Staphylococcus aureus*, fruit fly, *Arabidopsis thaliana*, and human. Secondary structural elements of $Cab2_{H337A}$ are shown above, while human PPCS [14] is shown below the aligned sequences. The conserved residues are colored in red, and the identical residues are highlighted in red. Orange residues represent the disordered regions (Met1–Thr37/Glu39; Ser229–Glu242, and Lys361–Lys365) in $Cab2_{H337A}$ structure. The partially disordered loop1, which reaches out to the adjacent monomer, is highlighted in green. The loop 2 (Leu310–Lys315), disordered in human and not conserved in *E. coli*, is highlighted as cyan. Residue Lys281 conserved in eukaryotic enzymes is colored in blue. The residues proposed to be important for CTP binding are marked by red stars. The highly conserved residue Asn97 marked by green triangle is important for the catalytic reaction. The strictly conserved residue Asp coordinated with the divalent metal ion is marked by blue quadrate.

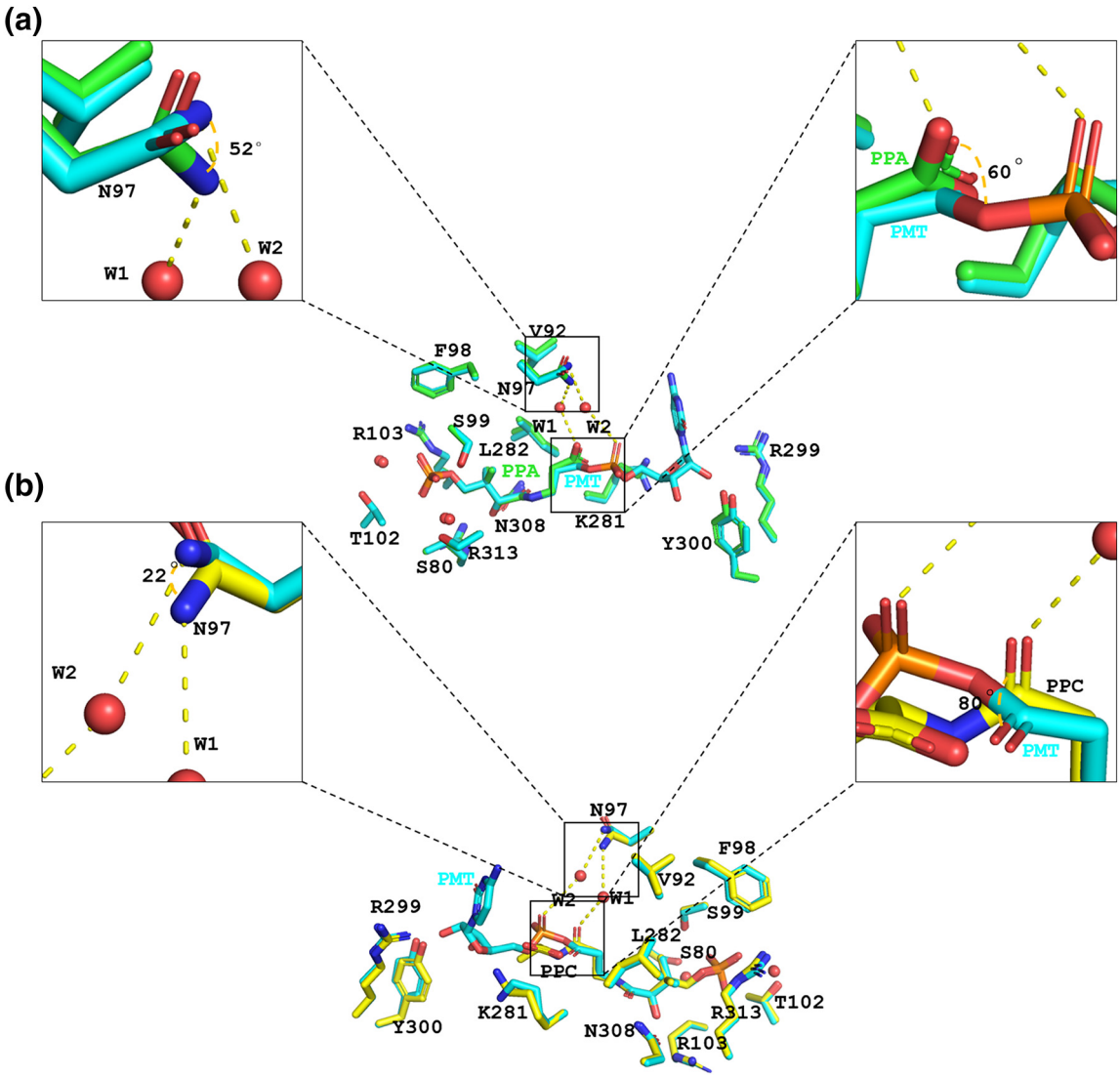

Fig. 5. Conformational changes of the active-site residue of $Cab2_{H337A}$ and ligands. The side chains of active-site residues and ligands are shown as sticks. Golden dashed lines represent hydrogen bonds. The residues and ligands are colored with green for $Cab2_{H337A}$–PPA, cyan for $Cab2_{H337A}$–PMT and yellow for $Cab2_{H337A}$–PPC. Comparison of the active-site residues and ligands in monomer A of the complex structures of (a) $Cab2_{H337A}$–PPA with $Cab2_{H337A}$–PMT and (b) $Cab2_{H337A}$–PMT with $Cab2_{H337A}$–PPC.

with the carboxyl group. The backbone amide of Leu282 and the backbone oxygen of Phe280 form hydrogen bonds with the carboxyl group and amino group of L-cysteine-moiety, respectively. The thiol of cysteine-moiety is oriented toward the hydrophobic cavity formed by Leu192, Leu208, Val212, and Leu264. The γ-amino group of Asn97 forms a water-mediated hydrogen bond through W1 (water 573 in monomer A and water 612 in monomer B) with carbonyl of PPA-moiety. Interestingly, these two water molecules lie at the same position as water 612 and water 644 in $Cab2_{H337A}$–PPA complex. Our enzymatic assays indicated that Cab2 could also utilize cystine *in vitro*. To further determine whether the thiol of cysteine attacks the activated carbonyl of PMT to generate PPC, we determined the structure of $Cab2_{H337A}$ in complex with PPS [16]. The PPS was generated *in situ* and presents in the complex structure as illustrated in Fig. 2b. Since the thiol is replaced by disulfide bond in PPS, the result of enzymatic assays and the complex structure demonstrated that PPC is formed by the nucleophilic attack of the amino group of cysteine to acyl group directly.

Comparison of Cab2 and PPCS enzymes from *E. coli* and human

To illuminate the catalytic mechanism, comparative analysis of Cab2 was performed with PPCS enzymes from human and ecCoaB from *E. coli*. It is clear from the

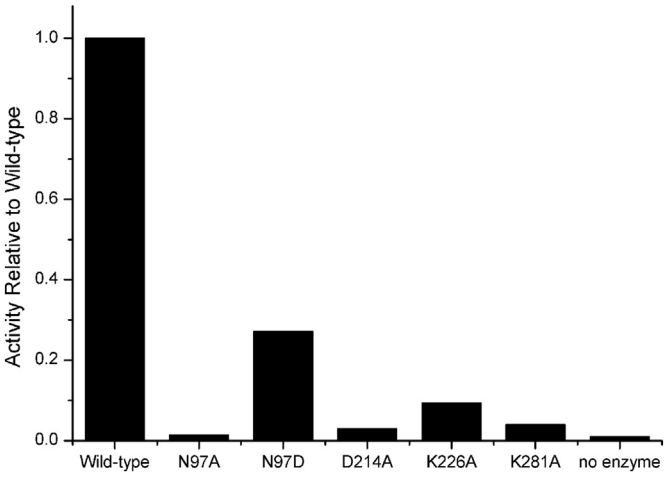

Fig. 6. Specific activities of various mutants relative to wild-type of Cab2.

sequence alignment that about 50 residues at the N-terminus and more than 10 residues in the middle of Cab2 are significantly different from the PPCS enzymes from human and *E. coli* (Fig. 3). Cab2 forms one α helix at the N-terminus and one strand β sheet in the middle. However, more than 30 residues at the N-terminus and more than 10 residues at the middle are disordered in our structures. These N-terminus disordered residues are far away from the active pocket, hence are unlikely associated with the enzymatic reaction and might be essential for the interaction with other CoA biosynthetic enzymes in yeast [12].

The structure alignments indicate that the major architectures are conserved among them (Fig. 4a, b) [14,15]. Overall structure of the enzymes represent tightly binding dimers linked by dimerization domains which are comprised of three regions as shown in Fig. S4. However, the second interaction region formed by helices and loops is not present in the ecCoaB. The last interface extending to the adjacent

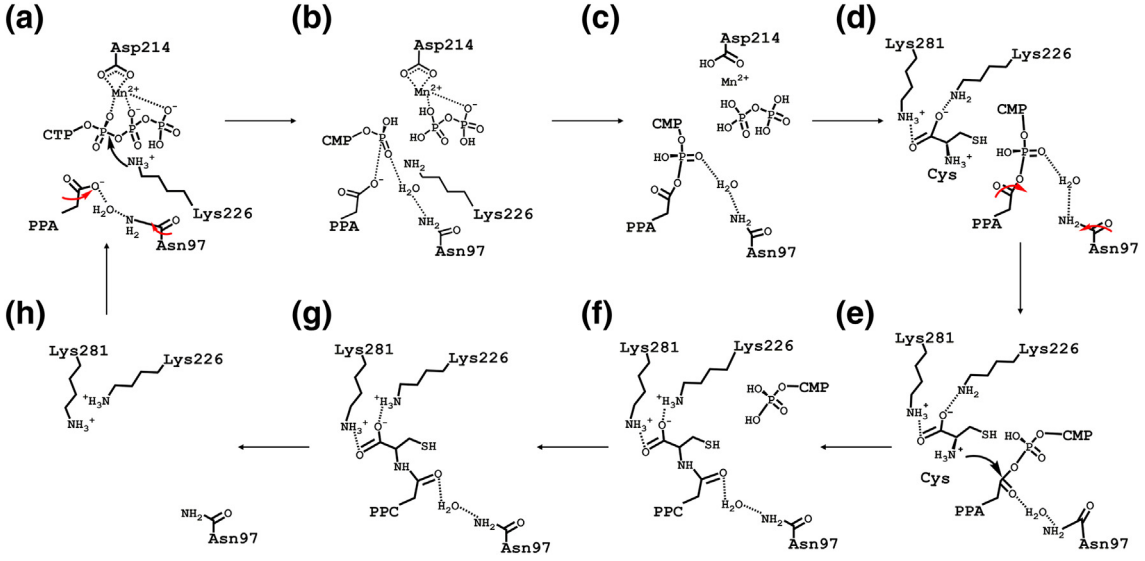

Fig. 7. Proposed catalytic mechanism of Cab2. Chemical structures were prepared using ChemDraw. The divalent metal ions (Mn^{2+}/Mg^{2+}) were represented by the Mn^{2+} in the figure. The rotations of carboxyl of PPA and γ-amino group of Asn97 were expressed by red arrows. Dashed lines represent the hydrogen bonds, salt bridges, and coordination bond. (a) PPA and CTP binding to the active site. The ε-amino of Lys226 donates a proton to make a nucleophilic attack on the α-phosphate of CTP. (b) The breaking of the bond between α- and β-phosphate, rotating the carboxyl of PPA, and formation of bond between PPA and α-phosphate. (c) The formation of PMT and leaving of pyrophosphate. (d) The binding of cysteine. (e) The rotating of carbonyl and CMP moiety of PMT. The amino group of cysteine nucleophilic attack exposed to carbonyl of PMT. (f) Formation of bond between PPA and cysteine and the breaking of bond between CMP and PPA-moiety. The leaving of CMP. (g) The leaving of PPC. (h) Ligand free Cab2.

subunit partially forms a disorder loop in all enzymes (yeast: 229–242; human: 192–202; *E. coli*: 290–299). Loop2, important for PPA binding in Cab2 is significantly different from ecCoaB and human PPCS (Fig. 3 and S5).

From the comparison of nucleotide binding sites of PPCS enzymes, it was clear that there is a noticeable difference in the base-interacting parts of eukaryotic and prokaryotic enzymes (Fig. 4c). The position of helix α7 and the preceding loop of Cab2 is similar to human PPCS while significantly different from ecCoaB (yeast: 259–270; human: 209–220; *E. coli*: 306–316, shown as ribbon in Fig. 4c and d). This region is important for cytosine binding in ecCoaB [15]. However, its deviation in Cab2 is responsible for less favorable binding to cytosine, which is in agreement with our ITC results that CTP has a lower binding affinity for Cab2 than ecCoaB (Figs. 1a and S1; Table S1). Different conformations of cytosine groups of CMP-moiety were observed in $Cab2_{H337A}$–PMT complex. The flexibility of the cytosine is probably due to large nucleotide binding site not filling optimally by cytosine. Consistent with the higher binding affinity and enzymatic activity of ATP than CTP to Cab2, this region likely plays an important role in the selection of ATP over CTP. A divalent metal ion (Ca^{2+} in *E. coli*; Mg^{2+} in *M. smegmatis*. PDB ID: 1U7W; 4QJI) is coordinated by α- and β-phosphates of CTP and highly conserved Asp residue in PPCS enzymes (yeast: Asp214; ecCoaB: Asp279; human PPCS: Asp183; *M. smegmatis*: Asp281; Figs. 3 and 4c) [15]. As Mn^{2+}/Mg^{2+} are essential for the enzymatic reaction in yeast, it was proposed that Mn^{2+}/Mg^{2+} occupies similar positions to Ca^{2+} in *E. coli* and Mg^{2+} in *M. smegmatis* PPCS. In addition, the pocket has several conserved positive charged residues, including Lys281 from Monomer A and Arg93 and Lys226 from the adjacent monomer in yeast (Figs. 3 and 4c). These residues are proposed to be important for binding of CTP [15]. We proposed that the negative charged phosphate groups of CTP were anchored at these positively charged residues in Cab2.

Proposed catalytic mechanism of Cab2

The PMT generated *in situ* and presenting in the active-site pocket in the PMT complex crystal demonstrates that CTP and PPA can bind concurrently and enzymatic reaction could proceed in the presence of Mn^{2+}/Mg^{2+}. From the structural comparison, we speculated that Mn^{2+}/Mg^{2+} and positive charged side chains around the phosphate groups in Cab2 contribute in deviating negative charges from the leaving pyrophosphate of CTP, which is beneficial for a nucleophilic attack.

Asn97, an extremely conserved residue throughout the PPCS enzymes (ecCoaB: Asn210; human PPCS: Asn59, Fig. 3), interact with the carboxyl group of PPA, the carbonyl of PPA-moiety of PMT, and α-phosphate of CMP-moiety of PPC through water-mediated hydrogen bonds (Fig. 2c–h). The mutant Asn210Asp of ecCoaB demonstrated significantly low catalytic activity *in vitro* [15]. The residue Asn97 was also proposed to be important for the enzymatic activity of Cab2 in yeast. From comparison with $Cab2_{H337A}$–PPA complex, it was clear that the γ-amino group of Asn97 in PMT complex rotates about 52° that is likely to take an applicable distance to interact with W2. In contrast, the carbonyl of PPA-moiety rotates about 60° to distance itself from the W1 and possibly to make the carboxyl of PPA close to the α-phosphate of CTP, simultaneously (Fig. 5a).

To evaluate the functional importance of the residues, which are proposed to be important for the catalytic reaction, we carried out enzymatic assays by using various mutants. The activity of enzymatic reaction was measured in the presence of 10 mM DTT, 1 mM L-cysteine, 800 μM PPA, 800 μM CTP, 1 mM $MnCl_2$, and 2.8 μg wild-type or various mutants of Cab2. As illustrated in Fig. 6, all mutants retain only a partial enzymatic activity relative to wild-type under the same condition. The $Cab2_{N97A}$ mutant retains the minimum activity (only about 1.4%) and the $Cab2_{N97D}$ mutant retains about 27.2% activity of wild-type, which are consistent with the previous reports that the conserved Asn residue was important for the activity of PPCS [10,20]. In addition, the residues of Asp214, Lys226, and Lys281 were also crucial for the activity of Cab2.

These considerations depict that the reaction starts while PPA and CTP bind to the active site (Fig. 7a). Similar to the pantothenate synthetase from *Mycobacterium tuberculosis*, a proton was proposed to makes a nucleophilic attack on the α-phosphate of CTP and contributes in leaving of the pyrophosphate [21]. Figure 4d illustrates that Lys226 acts as a general acid, which might be a proton donor, as it is essential for binding of phosphate groups, Moreover, ε-amino of Lys226 lies in close proximity to the phosphate group of CMP in PMT complex with a distance at 4.8 Å (5.9 Å in monomer B). The breaking of bond between α- and β-phosphates, rotating of the carboxyl of PPA, and the γ-amino group of Asn97 and the formation of bond between carboxyl of PPA and α-phosphate of CTP are immediately followed by the nucleophilic attack (Fig. 7b). A water-mediated hydrogen bond is formed between the phosphate group of CMP-moiety and the γ-amino group of Asn97 through W2 in order to stabilize the phosphate group (Fig. 7c).

In $Cab2_{H337A}$–PPC complex structure, the carboxyl group is stabilized by Lys281 from monomer A and Lys226 from the adjacent monomer (Figs. 2g–h and 7d). Aligned with the $Cab2_{H337A}$–PMT complex structure, the carbonyl of PPA-moiety rotates about 80° to the site which binds to W1 by hydrogen bond. In contrast, the γ-amino group of Asn97 in PPC complex rotates about 22° back to form a hydrogen bond with W1 (Fig. 5b). It was proposed that cysteine can make a nucleophilic attack on the carbonyl carbon of the

acyl-intermediate directly [16]. Moreover, the cysteine/cystine selectivity assays and the PPS complex structure demonstrate that the intermediate is attacked by the amino group of cysteine directly.

From these considerations, it is suggested that CMP-moiety is rotated to decrease the steric repulsions between the CMP-moiety and cysteine, while the carbonyl of the PPA-moiety is exposed to the amino group of cysteine (Fig. 7e). The positively charged side chains of Lys281 and Lys226 binding to the carboxyl of cysteine draw the negative charges toward the carboxyl, which is beneficial to the nucleophilic attack. The active amino group of cysteine makes a nucleophilic attack on the carbonyl carbon, followed by the formation of bond between PPA and cysteine, cleavage of the bond between CMP- and PPA-moiety, and CMP releasing (Fig. 7f). The imino group of cysteine-moiety is stabilized by the backbone nitrogen of Phe280 through hydrogen bond. The carbonyl of PPA-moiety forms a water-mediated hydrogen bond with the γ-amino group of Asn97 through W1 (Fig. 7g).

Materials and Methods

Protein expression and purification

The wild-type Cab2 from *Saccharomyces cerevisiae* was cloned into pET28a (Novagen) vector with an N-terminal 6× His tag fused. The Cab2 construct was transformed into *E. coli* Rosetta (DE3) cells (Stratagene), which were grown in 800 ml LB medium containing 60 mg L^{-1} kanamycin at 310 K. When the OD600 reached 0.8, the protein was overexpressed by inducted with 400 μM IPTG at 289 K for 16 h. Cells were harvested by centrifugation at 8000 rpm for 6 min at 281 K. The cell pellets were suspended in ice-cold buffer A [50 mM Tris–HCl (pH 8.0), 500 mM NaCl] and lysed by sonication. The supernatant was obtained by centrifugation at 12,000 rpm for 30 min at 277 K. The recombinant protein was purified by affinity chromatography using a Ni-NTA column (GE Healthcare, USA) and eluted with buffer A containing 400 mM imidazole. After concentration, the recombinant protein was further purified by gel filtration using Superdex 16/200 column (GE Healthcare, USA). Mutant proteins and CoaB (181–406) domain of coaBC from *E. coli* (ecCoaB) were recombined and purified as wild-type Cab2. Proteins were then concentrated using a Millipore concentrator (Amicon, USA). Finally, $Cab2_{H337A}$ was concentrated to 40 mg/ml in buffer B [50 mM Tris–HCl (pH 8.0), 15 mM NaCl) and buffer C [50 mM MES (pH 6.5), 15 mM NaCl] for crystallization experiments and wild-type Cab2 and ecCoaB were concentrated to 26 mg/ml in buffer D [50 mM Hepes (pH 7.3), 100 μM NaCl] for ITC assays.

PPA preparation

PPA was synthesized by Cab1 from pantothenate and ATP as reported previously [15]. Briefly, 5 ml calcium pantothenate (60 mM) was mixed with an equal volume of sodium phosphate (40 mM). The precipitate was removed by centrifugation at 12,000 rpm for 30 min at 277 K and sodium pantothenate (120 mM) was prepared. Sodium pantothenate (5 mM) was phosphorylated by PANK Cab1 (1 μM) in buffer containing 20 mM Tris–HCl (pH 8.0), 2.5 mM $MgCl_2$, and 5 mM ATP. After 1-h incubation with gently shaking (160 rpm) at 310 K, Cab1 was removed by ultrafiltration. The flow-through including PPA was lyophilized in the vacuum and stored at 193 K.

Isothermal titration calorimetry

Dissociation constant (K_D) values of PPA, CTP, and ATP to proteins were measured by Microcal PEAQ-ITC equipment (MicroCal Inc., USA) at 293 K. Briefly, 40 μl PPA, CTP, and ATP (600 μM) was injected into the sample cell containing ecCoaB (60 μM) or Cab2 (60 μM) in buffer D. Data obtained from ITC assay were fitted to one-site binding model via the MicroCal PEAQ-ITC analysis software (MicroCal Inc., USA).

Enzymatic assay

The Cab2 activity assays were performed at 310 K in a 100-μl reaction system. To uncover ligands specificity of Cab2, series enzymatic assays were performed in our study. To determine the metal selectivity, the activity of Cab2 was measured in the presence of 10 mM DTT, 1 mM L-cysteine, 800 μM PPA, 800 μM CTP, 2.8 μg Cab2, and 1 mM various metal ions ($MgCl_2$, $MnCl_2$, $CuCl_2$, $CaCl_2$, $FeCl_3$). To investigate the nucleotide selectivity of Cab2, the enzymatic activity was measured in the presence of 10 mM DTT, 1 mM L-cysteine, 800 μM PPA, 2.8 μg Cab2, and 800 μM $MgCl_2$, 2 mM CTP, or ATP. In order to further identify the L-cysteine/cystine/serine selectivity of Cab2, Cab2 was assayed in the presence of 10 mM DTT, 800 μM PPA, 2.8 μg Cab2, and 800 μM $MgCl_2$, 800 μM CTP, 5 mM L-cysteine, or serine. Except for the 10 mM DTT, the activity of 5 mM cystine containing reaction was measured under the same condition. The reactions were initiated by adding enzyme, and the mixture was incubated at 310 K for 30 min. The reaction was stopped by the addition of EDTA to a final concentration of 20 mM [22]. The product of pyrophosphate was measured using the pyrophosphate assay kit (MAK168, Sigma). Ten microliters of the master reaction mix was combined with equal volume of reaction mixture in 384-well plate. After incubation at 298 K for 10 min, the fluorescence intensity (λ_{ex} = 316 nm/λ_{em} = 456 m) was measured

on Synergy H1 (Biotek, USA) plate reader. To enable accurate quantitation, assays were done in duplicates.

Crystallization

Hanging-drop vapor diffusion method was applied to obtain crystals at 287 K by mixing 1.1 μl protein with an equal volume of reservoir solution. Optimized crystal of $Cab2_{H337A}$ was achieved in 100 mM Hepes (pH 7.0), 18% PEG 4000, and 150 mM $(NH_4)_2SO_4$.

Crystals of protein: PPA complex were obtained in 200 mM ammonium tartrate and 20% PEG 3350, after incubating 0.2 mM protein with 2 mM PPA and 4 mM CTP in buffer B for 2 h at 277 K.

In order to obtain protein complex with PMT, 0.2 mM protein was mixed with 2 mM PPA, 4 mM CTP, and 3 mM $MnCl_2$ in buffer B and incubated for 2 h at 277 K. Crystals were grown for diffraction in 200 mM potassium sodium tartrate and 20% PEG 3350.

To obtain the crystals of the protein complex with PPC, 0.2 mM protein was mixed with 2 mM PPA, 6 mM CTP, 8 mM L-cysteine, 2 mM DTT, and 3 mM $MnCl_2$ in buffer C. The mixture was incubated at 277 K for 2 h before crystallization. The crystals were gained under same crystallization condition as $Cab2_{H337A}$–PPA complex.

To acquire the crystals of the protein complex with PPS, which is the analogue of PPC, 0.2 mM protein was incubated with 2 mM PPA, 6 mM CTP, 8 mM cystine, and 3 mM $MnCl_2$ in buffer B for 2 h at 277 K before crystallization. The crystals were obtained at the same condition of PPC complex.

Data collection, structure determination, and refinement

For data collection, crystals of $Cab2_{H337A}$ were flashed-cooled in liquid nitrogen after immersing in the cryoprotectant composed of 15% (v/v) glycerol, while ligands containing crystals were cryoprotected in 20% (v/v) PEG 400 in the containing reservoir solution for few seconds. It should be noted that crystal of $Cab2_{H337A}$ in complex with PPC was soaked with 5 mM CTP and 10 mM L-cysteine for about 15 s before cooling. All diffraction data were collected at 100 K. Diffraction data for $Cab2_{H337A}$ and its complex with PMT and PPS were collected on beamline BL19U1 at SSRF (Shanghai Synchrotron Radiation Facility) at the wavelength of 0.97853 Å, while $Cab2_{H337A}$ compex with PPC was collected on BL18U1 at 0.97852 Å. Diffraction data for $Cab2_{H337A}$ complex with PPA were collected at 1.5417 Å using Cu X-ray generated by MicroMax-007 rotating-anode X-ray source at in-house instrument (Rigaku K2000, USA). All data collected were indexed, integrated, and scaled using the HKL2000 software package [23]. Initial phases were determined by molecular replacement method using the Molrep from CCP4i software package and human PPCS (PDB ID: 1P9O) as a search model [14,24,25]. The structures were refined using Refmac5 for restrained refinement and Coot for manual modulation alternately [26,27]. Since the structures of PPC and PPS ligands were absent from the PDB database, structure restraints for PPC and PPS were produced using the *eBLOW* contained in *PHENIX* software package [28,29]. The structure models were validated using the PROCHECK [30]. All figures containing structures were prepared by *PyMol* [31]. Data collection and model refinement data are shown in Tables 1 and S2.

Accession numbers

The atomic coordinates have been deposited in the Protein Data Bank (PDB) (codes: $Cab2_{H337A}$, 6AI8; complex with PPA, 6AI9; complex with PMT, 6AIK; complex with PPC, 6AIM; complex with PPS, 6AIP).

Acknowledgments

This work was supported by the Chinese National Natural Science Foundation (Grant Nos. U1632124 to L. N., 31270770 to Z. Z., and 31621002 to L. N.), the Chinese Ministry of Science and Technology (Grant Nos. 2017YFA0503600 to L. N., 2017YFA0504903 to L. N., and 2012CB917200 to Z. Z.), and the China Postdoctoral Science Foundation (Grant No. 2017M622012 to M. Z.).

We thank the staff at beamline BL18U and BL19U of the Shanghai Synchrotron Radiation Facility for assistance with data collection. We thank Dr. Jiyuan Ke for assistance with critical comments and manuscript revision.

Author Contributions: Peiyi Zheng conceptualized the project. Peiyi Zheng and Mengying Zhang were responsible for data curation and formal analysis of the experiments. Yongxiang Gao and Maikun Teng provided some suggestions during experiments. Zhongliang Zhu, Mengying Zhang, and Liwen Niu supervised the project. Project was supported under the fundings of Zhongliang Zhu, Mengying Zhang, and Liwen Niu. Hejun Liu and Jian Yue validated the data. Peiyi Zheng wrote the original draft. Muhammad Hidayatullah Khan, Hejun Liu, Yuping Jin, and Jian Yue reviewed and edited the article.

Conflict of Interest: The authors declare that they have no conflict of interest.

Appendix A. Supplementary data

Supplementary data to this article can be found online at https://doi.org/10.1016/j.jmb.2019.01.012.

Received 1 October 2018;
Received in revised form 6 January 2019;
Accepted 8 January 2019
Available online 14 January 2019

Keywords:
Cab2;
catalytic mechanism;
CoA biosynthesis;
crystal structure;
PPCS

Abbreviations used:
PPCS, phosphopantothenoylcysteine synthetase; PPA, 4′-phosphopantothenate; Cab2, coenzyme A biosynthesis protein 2; PMT, 4′-phosphopantothenoyl-CMP; PPS, phosphopantothenoylcystine; PANK, pantothenate kinase; PPAT, phosphopantetheine adenylyl transferase; DPCK, dephosphocoenzyme A kinase; ITC, isothermal titration calorimetry.

References

[1] F. Lipmann, N.O. Kaplan, G.D. Novelli, Chemistry and distribution of the coenzyme for acetylation (coenzyme A), Fed. Proc. 6 (1 Pt 2) (1947) 272.
[2] R. Leonardi, et al., Coenzyme A: back in action, Prog. Lipid Res. 44 (2–3) (2005) 125–153.
[3] G.M. Brown, The metabolism of pantothenic acid, J. Biol. Chem. 234 (2) (1959) 370–378.
[4] G. Annesi, et al., Mutational analysis of COASY in an Italian patient with NBIA, Parkinsonism Relat. Disord. 28 (2016) 150–151.
[5] A. Iuso, et al., Mutations in PPCS, encoding phosphopantothenoylcysteine synthetase, cause autosomal-recessive dilated cardiomyopathy, Am. J. Hum. Genet. 102 (6) (2018) 1018–1030.
[6] E. Strauss, et al., Phosphopantothenoylcysteine synthetase from *Escherichia coli*—identification and characterization of the last unidentified coenzyme A biosynthetic enzyme in bacteria, J. Biol. Chem. 276 (17) (2001) 13513–13516.
[7] T.P. Begley, C. Kinsland, E. Strauss, The biosynthesis of coenzyme A in bacteria, Vitam. Horm. 61 (61) (2001) 157–171.
[8] M. Daugherty, et al., Complete reconstitution of the human coenzyme A biosynthetic pathway via comparative genomics, J. Biol. Chem. 277 (24) (2002) 21431–21439.
[9] J. Yao, G.D. Dotson, Kinetic characterization of human phosphopantothenoylcysteine synthetase, Biochim. Biophys. Acta 1794 (12) (2009) 1743–1750.
[10] T. Kupke, P. Hernandez-Acosta, F.A. Culianez-Macia, 4′-Phosphopantetheine and coenzyme A biosynthesis in plants, J. Biol. Chem. 278 (40) (2003) 38229–38237.
[11] J. Olzhausen, S. Schubbe, H.J. Schuller, Genetic analysis of coenzyme A biosynthesis in the yeast *Saccharomyces cerevisiae*: identification of a conditional mutation in the pantothenate kinase gene CAB1, Curr. Genet. 55 (2) (2009) 163–173.
[12] J. Olzhausen, et al., Molecular characterization of the heteromeric coenzyme A-synthesizing protein complex (CoA-SPC) in the yeast *Saccharomyces cerevisiae*, FEMS Yeast Res. 13 (6) (2013) 565–573.
[13] J.W. Yao, J.D. Patrone, G.D. Dotson, Characterization and kinetics of phosphopantothenoylcysteine synthetase from *Enterococcus faecalis*, Biochemistry 48 (12) (2009) 2799–2806.
[14] N. Manoj, et al., Structure of human phosphopantothenoylcysteine synthetase at 2.3 angstrom resolution, Structure 11 (8) (2003) 927–936.
[15] S. Stanitzek, et al., Structural basis of CTP-dependent peptide bond formation in coenzyme A biosynthesis catalyzed by *Escherichia coli* PPC synthetase, Structure 12 (11) (2004) 1977–1988.
[16] E. Strauss, Coenzyme A biosynthesis and enzymology, in: H.-W. Liu, L. Mander (Eds.), Comprehensive Natural Products II, Elsevier 2010, pp. 351–410.
[17] E. Strauss, T.P. Begley, The selectivity for cysteine over serine in coenzyme A biosynthesis, Chembiochem 6 (2) (2005) 284–286.
[18] R.C. Edgar, MUSCLE: multiple sequence alignment with high accuracy and high throughput, Nucleic Acids Res. 32 (5) (2004) 1792–1797.
[19] X. Robert, P. Gouet, Deciphering key features in protein structures with the new ENDscript server, Nucleic Acids Res. 42 (Web Server issue) (2014) W320–W324.
[20] T. Kupke, et al., Molecular characterization of lantibiotic-synthesizing enzyme EpiD reveals a function for bacterial Dfp proteins in coenzyme A biosynthesis, J. Biol. Chem. 275 (41) (2000) 31838–31846.
[21] S.S. Wang, D. Eisenberg, Crystal structures of a pantothenate synthetase from *M. tuberculosis* and its complexes with substrates and a reaction intermediate, Protein Sci. 12 (5) (2003) 1097–1108.
[22] J. Kottur, D.T. Nair, Pyrophosphate hydrolysis is an intrinsic and critical step of the DNA synthesis reaction, Nucleic Acids Res. 46 (12) (2018) 5875–5885.
[23] Z. Otwinowski, W. Minor, Processing of X-ray diffraction data collected in oscillation mode, Macromol. Crystallogr. Pt. A 276 (1997) 307–326.
[24] M.D. Winn, et al., Overview of the CCP4 suite and current developments, Acta Crystallogr. D Biol. Crystallogr. 67 (Pt 4) (2011) 235–242.
[25] A. Vagin, A. Teplyakov, Molecular replacement with MOLREP, Acta Crystallogr. Sect. D Biol. Crystallogr. 66 (2010) 22–25.
[26] G.N. Murshudov, et al., REFMAC5 for the refinement of macromolecular crystal structures, Acta Crystallogr. D Biol. Crystallogr. 67 (Pt 4) (2011) 355–367.
[27] P. Emsley, K. Cowtan, Coot model-building tools for molecular graphics, Acta Crystallogr. D Biol. Crystallogr. 60 (2004) 2126–2132.
[28] N.W. Moriarty, R.W. Grosse-Kunstleve, P.D. Adams, Electronic Ligand Builder And Optimization Workbench (eLBOW): a tool for ligand coordinate and restraint generation, Acta Crystallogr. D Biol. Crystallogr. 65 (2009) 1074–1080.
[29] P.D. Adams, et al., PHENIX: a comprehensive Python-based system for macromolecular structure solution, Acta Crystallogr. D Biol. Crystallogr. 66 (2010) 213–221.
[30] R.A. Laskowski, et al., Procheck—a program to check the stereochemical quality of protein structures, J. Appl. Crystallogr. 26 (1993) 283–291.
[31] W.L. Delano, PyMol, http://www.pymol.org 2002.